IEEE Access
Multidisciplinary | Rapid Review | Open Access Journal

Received 12 December 2023, accepted 26 December 2023, date of publication 28 December 2023,
date of current version 4 January 2024.

Digital Object Identifier 10.1109/ACCESS.2023.3347779

RESEARCH ARTICLE

Social Force Model-Based Adaptive Parameters Collision Avoidance Method Considering Motion Uncertainty of the Pedestrian

YAN ZHANG, XINGGUO ZHANG, YOHEI FUJINAMI, AND PONGSATHORN RAKSINCHAROENSAK

Department of Mechanical Systems Engineering, Tokyo University of Agriculture and Technology, Tokyo 184-8588, Japan

Corresponding author: Yan Zhang (s212249y@st.go.tuat.ac.jp)

ABSTRACT In typical traffic scenarios such as non-signalized roads or shared spaces where vehicles and pedestrians interact without clear separations. The interaction distance between objects is usually shorter due to the simultaneous motion of road users. Pedestrian-crossing scenarios in these areas make the scenario complex due to the unpredictability of the pedestrians intention and the need to balance between safety, comfort, and time consumption. To address this collision avoidance(CA) problem, a novel strategy using Social Force Model (SFM)-based adaptive parameters was proposed. The interaction system between the ego vehicle and the pedestrian was simplified as a Markov process to adopt the SFM-based dynamic model, and the validity of this simplification was demonstrated using real-world driving data. Based on the current state of the interaction system that consists of vehicle and pedestrian, this research adopted the optimal parameters that were generated by particle swarm optimization (PSO) to generate optimal parameters for the SFM-based vehicle dynamic model, which helps the vehicle avoid pedestrians with random motion. The proposed method was validated through bench testing, and the results showed that the proposed method balanced the safety, comfort, and time consumption requirements during the CA process in the studied scenario.

INDEX TERMS Collision avoidance, social force model, autonomous vehicle, pedestrian-vehicle interaction.

I. INTRODUCTION

For intelligent control system or advanced driver assistance systems (ADAS) that are equipped in highly automated vehicles. Their main function are to maintain safer driving for both drivers and pedestrians [1], [2], [3], especially on non-signalized road. In some countries in Southeast Asia, electric bikes are more and more involved in the interaction of traffic flow due to their convenience and quickness [4]. Users of this type of transportation blur the line between vehicles and pedestrians, as all traffic participants can move freely in the same space. At the same time, shared space, which is used to increase the attractiveness of people traveling to public spaces, is more and more mentioned in western countries by urban design as an alternative to traditional designs [5], [6]. The shared space, like mixed traffic, is a concept that promotes a sense of vigilance and responsibility by reducing demarcations and any physical distinction between the streets and pedestrian areas [7]. Facing this kind of traffic section, such as a scenario shown in Fig. 1,which was a video frame collected by Smart Mobility Research Center (SMRC) [8], drivers need to carefully assess the collision risk although driving speed is relatively low. And in such non-signalized areas, the moving priority of pedestrians is usually not very high, which means vehicles do not need to completely stop to wait for the pedestrians to pass. Therefore, when the motion of the pedestrian is certain, or in other words the moment when the pedestrian-crossing is stochastic from the perspective of drivers and taking into account the need of saving commute time or quickly passing through similar areas with uncertain risk, drivers or control agents need to balance of keeping relative higher velocity and ensuring proper safety distance during avoidance process.

The associate editor coordinating the review of this manuscript and approving it for publication was P. Venkata Krishna.

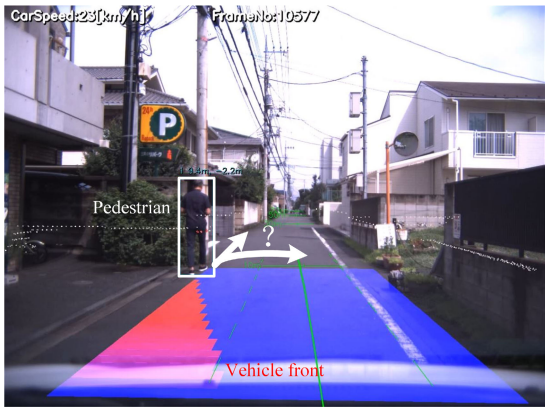

FIGURE 1. Possible routes choice for the pedestrian.

Focusing on such collision avoidance(CA) problems, a possible solution is to establish interaction relations between pedestrians and vehicles. A lot of research has been conducted to analyze pedestrian intention and vehicle-pedestrian interaction [9], [10], [11]. In [12] and [29], based on a statistical analysis of pedestrian behavior, a statistical framework to assess the risk of passing a non-signalized intersection for vehicles was established. Also, a predictive risk metric when a pedestrian appears was given quantitatively based on the pedestrian-aware risk model. The prediction of the pedestrian's motion was also adopted in [37]. In [13], Long Short Term Memory (LSTM) modules based recurrent neural networks were adopted to make a pedestrian intent prediction. However, the prediction was based solely on the motion trajectory of the pedestrian. The above research mainly focused on the risk assessment of pedestrian crossing road intention. However, it is still difficult to indicate the pedestrian's trajectory in the actual vehicle-pedestrian interaction. Also, some research focused directly on the pedestrian behavior or motion. And the social force model (SFM) is the most used method for modeling users of such shared space in micro-simulation and has been continually improved and modified since its first introduction [14]. Kretz et al. analytically solved the SFM resultant equations for very simple cases and provided helpful comments on model calibration [15]. Besides, not all researches focus on the interactions among pedestrians. Dias et al. explored the applicability of an SFM based microscopic simulation model for personal mobility vehicles and multiple pedestrians in mixed traffic [16]. Based on fundamental patterns of multi-pedestrian interaction with a low speed vehicle (front, back, and lateral interaction in open space), Yang et al. proposed an SFM-based vehicle-pedestrians interaction model, and this model was calibrated by the genetic algorithm (GA) based on trajectory data of the same vehicle-pedestrian interaction patterns from controlled experiments [17].

At the same time, there are also some CA strategies for vehicle controllers [18]. Some ADAS that aims to help drivers avoid collision risks have been developed. One of the main features of ADAS is the CA system. A sufficient CA architecture usually encompasses threat assessment, path planning, and path tracking strategies [19]. There are at least two common types of CA design control architecture that have been proposed and implemented. For example, a multi-layer CA system [20], which contains both a trajectory re-planning layer and a tracking layer [21], was proposed for active CA. This is the usual type of CA implementation and is also known as a guidance and navigation control system [22]. Besides, optimization algorithms based on different mathematical theories have also been proposed. Cheng et al. proposed virtual flu-id-flow-model based lane-keeping integrated with a collision avoidance control system to realize the function of both lane-keeping and collision avoidance [23]. The predictive nature and constraint handling capabilities of model predictive control (MPC) make it an attractive framework for leveraging these new technologies. So, MPC was also adopted in CA [24], [25], [38], [39]. A machine learning approach, such as the artificial neural network [26], [41] and collision cone approach [27] were also used for designing CA strategies. In addition, MPC combined with the SFM-based pedestrian model to create a more realistic interactive scenario was proposed by Yang et at., which also showed the potential of extending the method to address more complex vehicle-pedestrian interaction situations [28]. Besides, in [30], Shen et al. considered comfortable driving and proposed a control framework for Connected and Automated Vehicles(CAVs) to approach the signalized intersections with good driving comfort. Besides, vehicle risk assessment methods were also proposed to control a vehicle to keep the presented lane and avoid a collision that may be caused by a road object [40].

However, the previous research that developed CA strategies for autonomous vehicles may focus on the ego vehicle itself too much, less considering the dynamic of obstacles. For most research mentioned above, the motion of the obstacle was known in advance, such as being fixed in one position or moving along a predetermined trajectory by a given speed profile. Although other research, such as [4] and [28], adopted SFM for more realistic obstacle movement, there was also no randomness in the proposed SFM, which means the motion of obstacles can be predicted accurately in such researches. But, when considering the individual difference among pedestrians and the nuances of different shared space (like ages of pedestrians or visibility of area), the precise motion prediction of pedestrians is difficult to achieve, which also can be found in the results of research on modelings for similar mixed traffic scenarios, such as [17]. Thus, in this paper, we considered the uncertainty of pedestrians motion and proposed a novel SFM-based adaptive parameters method to help ego vehicle make avoidance without motion prediction of pedestrian, just by the force balance. The main contribution of this work is as follows:

- The Markov process was adopted to simplify the vehicle-pedestrian interaction system. The rationality of the simplification was illustrated by real driving data.

- A novel SFM-based adaptive parameters CA method for the ego vehicle was proposed when considering the uncertain motion of the pedestrian.

The rest of this paper is organized as follows: the problem formulation is presented in detail in section II. Section III establishes both the SFM-based pedestrian and vehicle dynamic model. Then the proposed method for vehicle's safe and quick passing is illustrated in section IV. A bench test is carried out to verify the proposed method in section V. Section VI is the conclusion.

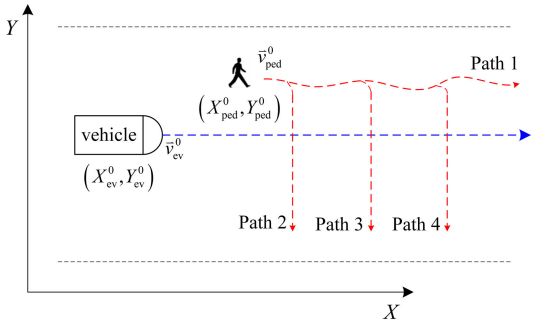

FIGURE 2. The scenario modeling of Fig.1.

II. PROBLEM DESCRIPTION

A. SCENARIO

This paper addresses the scenario illustrated in Fig. 2, where the ego vehicle moves forward in the same direction as a pedestrian. In Fig. 2, the Cartesian coordinates are defined by X and Y, respectively. Superscript 0 represents the initial states or parameters and subscript ped is the abbreviate of pedestrian where ev represents the ego vehicle. The future motion of the pedestrian is qualitatively defined as the following four possible realizations:

path 1: The pedestrian walks straightly without changing direction. In this case, the ego vehicle does not need to take on avoidance operation.

path 2 or 4: The crossing road behavior of the pedestrian is too early (or too late), and the ego vehicle has not approached yet (already passed). And in this case, the ego vehicle does not need to take avoidance operation as well.

path 3: If the ego vehicle does not avoid the pedestrian in time, the minimum distance between them will be smaller than a threshold safety distance (defined as $\min D_{\text{safe}}$ in the following sections) that indicates whether the collision avoidance process is safe or not. In this case, the ego vehicle must yield to avoid danger.

B. PROBLEM FORMULATION

With the above analysis, In the case of the pedestrian in paths 1, 2, and 4, the ego vehicle just needs to follow the initial trajectory and speed, which is considered the optimal operation when facing a pedestrian with potential crossing road intention. However, appropriate collision avoidance maneuverings in the case of path 3 need to be further discussed.

Considering reducing time consumption and maintaining passenger comfort, the purpose of this paper is to provide avoidance maneuvering for the ego vehicle under the requirements of safety, quick passing, and slight steering. As shown in Fig.2, the available information at time t is listed as:

(1) The current velocity and position of the ego vehicle: v_{ev}^t and $P_{\text{ev}}^t = [X_{\text{ev}}^t, Y_{\text{ev}}^t]$;

(2) The current velocity, position and yaw angle of the pedestrian: v_{ped}^t, $P_{\text{ped}}^t = [X_{\text{ped}}^t, Y_{\text{ped}}^t]$ and δ_{ped}^t.

δ_{obs}^t is the observation of δ_{ped}^t by vehicle sensors, which is used for judgment of ego vehicle that which path the pedestrian will choose:

$$\delta_{\text{obs}}^t \begin{cases} \in [-\delta_{\text{ped}}^{\text{thr}}, \delta_{\text{ped}}^{\text{thr}}], & \text{path 1} \\ \leq -\delta_{\text{ped}}^{\text{thr}}, & \text{path2 - 4} \end{cases} \tag{1}$$

Besides, the interaction between the ego vehicle and the pedestrian is essential. As the ego vehicle and the pedestrian are both the participants of traffic flow, the behavior of the participants is not only determined by their own will, but is usually influenced by the surrounding environment. Taking the pedestrian that decides to cross the road currently as an example, shown in Fig.3.

In Fig.3, the pedestrian, shown as green circle, is fixed currently as the shown state $\left(P_{\text{ped}}^{\text{now}}, v_{\text{ped}}^{\text{now}}\right)$. The ego vehicle, shown as triangle, owns different possible states that follow:

$$\begin{cases} \left\| P_{\text{ped}}^{\text{now}} - P_{\text{ev}}^1 \right\|_2 < \left\| P_{\text{ped}}^{\text{now}} - P_{\text{ev}}^2 \right\|_2 \\ v_{\text{ped}}^1 < v_{\text{ped}}^2 \end{cases} \tag{2}$$

Fig.3 gives the possible path choices for pedestrian-crossing when the pedestrian faces the vehicle owning different states. A pedestrian path that is with more time consuming, such as the path with red color, means the pedestrian slows his speed down for a safe crossing. When a pedestrian faces a closer or faster oncoming vehicle, the pedestrian will change its future his future behavior. Previous works proposed some methods to describe this kind of interaction and most of them were based on SFM [14], [15], [16], [17].

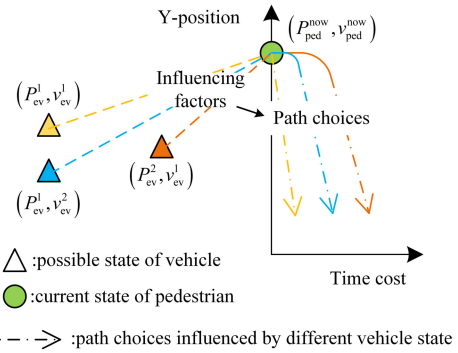

FIGURE 3. Possible path choices of pedestrian influenced by vehicle with different state.

Therefore, the states of these two participants are integrated as one system state which is written as:

$$\mathbb{S}^t = \left(\mathbb{S}_{\text{ev}}^t, \mathbb{S}_{\text{ped}}^t\right) \tag{3}$$

where $\mathbb{S}_{\text{ev}}^t = \left[P_{\text{ev}}^t, v_{\text{ev}}^t\right]$ and $\mathbb{S}_{\text{ped}}^t = \left[P_{\text{ped}}^t, v_{\text{ped}}^t\right]$ are the state of the ego vehicle and the pedestrian at current time t, respectively.

Assumption 1: The CA process of the interactive system consisting of the ego vehicle and the pedestrian follows the Markov process.

Generally, the whole CA process should be considered. However, when the future trajectory of the pedestrian follows an unknowable profile and is stochastic, the future state of the interaction system can be described by a transition probability matrix based on the current state, which is simplified as a Markov process. And Markov process has been adopted by many similar traffic processes [31], [32], [33], [34].

1) RATIONALITY OF ASSUMPTION 1 IN THIS STUDY

Although some previous research used the Markov process to illustrate similar traffic processes, they rarely justified the use of the Markov process.

To catch the key to improving safety driving by analyzing the interaction of ego vehicle and other traffic participants, some traffic data collected by our SMRC is adopted [8].

In this study, interaction events between pedestrians and the ego vehicle on a non-signalized road are used for illustration. The record signals include the following items:

- Video data containing cumulative frames and running time during interactions on the non-signalized road;
- Time series of vehicle lateral acceleration $a_{\text{ev}}^y(\cdot)$;
- Time series of lateral distance between ego vehicle and the $i-th$ pedestrian $d_{\text{ev2p}}^{y,i}(\cdot)$.

5 typical time series data sets consist of $a_{\text{ev}}^y(\cdot)$ and $d_{\text{ev2p}}^{y,i}(\cdot)$ are selected and used for correlation analysis. The collected data is shown in Fig.4. (In order to show concisely, here we only give the image of one data set in the total 5 sets, because their distributions are similar.)

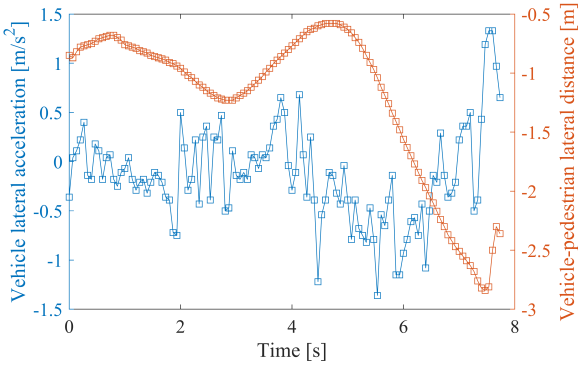

FIGURE 4. The time series of vehicle lateral acceleration and corresponding vehicle-pedestrian distance.

Fig. 4 shows some correlation in the time domain between a_{ev}^y and $d_{\text{ev2p}}^{y,i}$. The cross-correlation sequence of two joint stationary stochastic processes x_n, y_n was given by [36] as follows:

$$\hat{R}_{xy}(m) = \begin{cases} \sum_{n=0}^{N-m-1} x_{n+m} y_n^*, & m \geqslant 0; \\ \hat{R}_{yx}^*(-m), & m < 0 \end{cases} \tag{4}$$

where N is the length of time series data and $*$ denotes complex conjugation. The Eq.(4) can only estimate the sequence because, in practice, only a finite segment of one realization of the infinite-length random process is available. In general, the correlation function requires normalization to produce an accurate estimate by the following equation:

$$\hat{R}_{xy,\text{coeff}}(m) = \frac{1}{\sqrt{\hat{R}_{xx}(0)\,\hat{R}_{yy}(0)}} \hat{R}_{xy}(m) \tag{5}$$

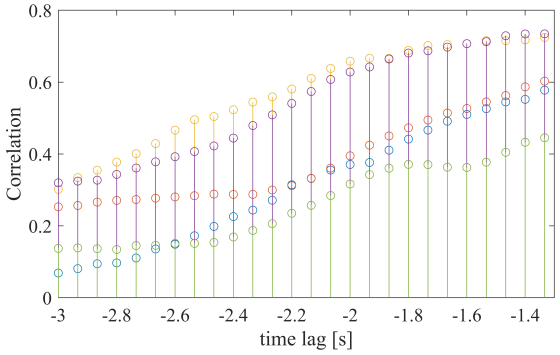

FIGURE 5. Normalization correlation analysis of vehicle-pedestrian interaction events.

And the results are shown in Fig.5. It shows that:

- As the correlation between the a_{ev}^y and $d_{\text{ev2p}}^{y,i}$ increases as the time delay decreases, it shows that the input of lateral acceleration directly affects the vehicle-pedestrian distance. The lateral acceleration is caused by the vehicle steering wheel angle which is considered system input, and the vehicle-pedestrian distance is the system state. So, the vehicle-pedestrian interaction system state of next time is transformed by the current system state and the system input.
- The correlation between the two sets of data drops sharply as the time delay increases, which means earlier historical input of lateral acceleration has little influence in the current state. This feature can be approximated as a non-aftereffect.

And the above analysis shows the rationality of approximating the vehicle-pedestrian system as a Markov process. Actually, from physical-view consideration, the future behavior of pedestrians and drivers, such as crossing road or accelerating/decelerating vehicles, is also mainly based on the current positions and respective velocity.

According to Assumption 1, the transition function of the interactive system could be established as:

$$\begin{cases} p_{\text{ev}}\left(\mathbb{S}_{\text{ev}}^{t+1} \middle| \mathbb{S}^t, \ldots, \mathbb{S}^0\right) = p_{\text{ev}}\left(\mathbb{S}_{\text{ev}}^{t+1} \middle| \mathbb{S}^t\right) \\ p_{\text{ped}}\left(\mathbb{S}_{\text{ped}}^{t+1} \middle| \mathbb{S}^t, \ldots, \mathbb{S}^0\right) = p_{\text{ped}}\left(\mathbb{S}_{\text{ped}}^{t+1} \middle| \mathbb{S}^t\right) \end{cases} \tag{6}$$

where p_{ev} and p_{ped} are the transition function of ego vehicle and the pedestrian, respectively.

Furthermore, the accessible maneuver for the ego vehicle during CA process is defined as a set of steering and acceleration in x-direction:

$$\mathbf{m}_{ev}^{t} = \left(\delta_{ev}^{t}, a_{ev}^{x,t}\right) \tag{7}$$

where δ_{ev}^{t} is the steering wheel angle at time t and $a_{ev}^{x,t}$ represents the acceleration in x-direction at time t. And the velocity v_{ev}^{t}, acceleration $a_{ev}^{x,t}$, and steering wheel angle δ_{ev}^{t} are within the proper bounds:

$$v_{ev}^{t} \in \left[0, v_{ev}^{\max}\right], \quad \forall t \in (t_0, t_{end}) \tag{8}$$
$$a_{ev}^{t} \in \left[-a_{ev}^{\max}, a_{ev}^{\max}\right], \quad \forall t \in (t_0, t_{end}) \tag{9}$$
$$j_{ev}^{t} \in \left[-j_{ev}^{\max}, j_{ev}^{\max}\right], \quad \forall t \in (t_0, t_{end}) \tag{10}$$
$$\delta_{ev}^{t} \in \left[-\delta_{ev}^{\max}, \delta_{ev}^{\max}\right], \quad \forall t \in (t_0, t_{end}) \tag{11}$$
$$\Delta\delta_{ev}^{t} \in \left[-\Delta\delta_{ev}^{\max}, \Delta\delta_{ev}^{\max}\right], \quad \forall t \in (t_0, t_{end}) \tag{12}$$

where j_{ev}^{t} and $\Delta\delta_{ev}^{t}$ are the jerk of acceleration and steering wheel angle at the current time, respectively. t_0 and t_{end} are the time when CA process starts and ends, respectively. Noticing that the lower bound of velocity is posed equally to zero in order to avoid unwanted backward movements. The bounds of a_{ev}^{t} and δ_{ev}^{t} are set to ensure that the trajectory of the vehicle is within a reasonable range in the real world. At the same time, the limits of change rates for the a_{ev}^{t} and δ_{ev}^{t} are used to reduce impact.

Besides, some limits are added to the pedestrian for the rationality of the movement as well:

$$v_{ped}^{t} \in \left[0, v_{ped}^{\max}\right], \quad \forall t \in (t_0, t_{end}) \tag{13}$$
$$a_{ped}^{t} \in \left[-a_{ped}^{\max}, a_{ped}^{\max}\right], \quad \forall t \in (t_0, t_{end}) \tag{14}$$

Considering the state $\mathbb{S}^{t+1}$ is decided by $\mathbb{S}^{t}$ and the maneuver m_{ev}^{t}, the transition function is updated as:

$$p\left(\mathbb{S}^{t+1} \middle| \mathbb{S}^{t}\right) \rightarrow p\left(\mathbb{S}^{t+1} \middle| \mathbb{S}^{t}, \mathbf{m}_{ev}^{t}\right) \tag{15}$$

The choices of different maneuver for the ego vehicle bring different transition possibilities based on the same current state of the interaction system. As shown in Fig.6, (a) of Fig.6 represents the current system state, that is defined as $\mathbb{S}^0$. The pedestrian is shown as a circle while the ego vehicle is simplified as a triangle. Considering two different maneuver for the ego vehicle which are $\mathbf{m}_{ev}^{1}$ and $\mathbf{m}_{ev}^{2}$, and in $\mathbf{m}_{ev}^{2}$, the acceleration $a_{ev}^{x,2}$ is larger than that of $\mathbf{m}_{ev}^{1}$. Then, the possibility of reaching the next states $\mathbb{S}^1$ and $\mathbb{S}^2$ will be different:

$$\begin{cases} p\left(\mathbb{S}^1 \middle| \mathbb{S}^0, \mathbf{m}_{ev}^{1}\right) \gg p\left(\mathbb{S}^2 \middle| \mathbb{S}^0, \mathbf{m}_{ev}^{1}\right) \\ p\left(\mathbb{S}^1 \middle| \mathbb{S}^0, \mathbf{m}_{ev}^{2}\right) \ll p\left(\mathbb{S}^2 \middle| \mathbb{S}^0, \mathbf{m}_{ev}^{2}\right) \end{cases} \tag{16}$$

The larger acceleration may bring farther moving distance for vehicle and greater avoidance for pedestrian, which means the possibility of reaching state $\mathbb{S}^2$ in (c) of Fig.6 is larger than that of $\mathbb{S}^1$ when taking maneuver m_{ev}^{2} under the same initial state $\mathbb{S}^0$. However, there is still some possibility of reaching $\mathbb{S}^1$ when taking m_{ev}^{2}, such as $a_{ev}^{x,1}$ is the upper limit of current state $\mathbb{S}^0$. Fig.6 and Eq.(16) are just established to explain that different maneuver taken by the ego vehicle may lead to different interaction system states of the next time step, and this is the reason for modifying the transition possibility function as Eq.(15).

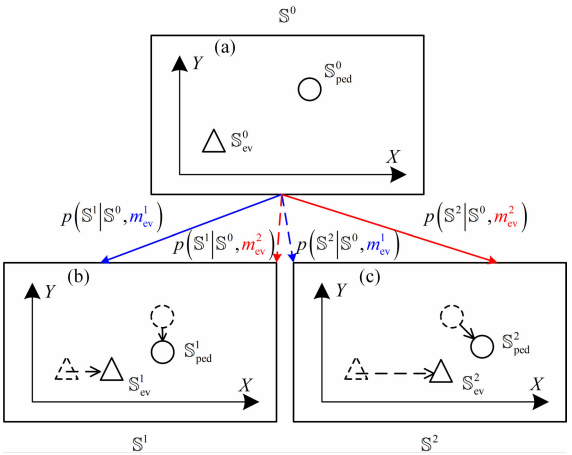

FIGURE 6. Different probabilistic state trajectories of the interactive system based on different $\mathbf{m}_{ev}^{t}$.

Furthermore, for the system state $\mathbb{S}^t$, we aim to find the optimal maneuver $m_{ev}^{*,t}$ that is accessible currently to reach the optimal state $\mathbb{S}^{*,t+1}$. So, a reward function is established to evaluate the currently chosen maneuver m_{ev}^{t}:

$$\begin{aligned} r\left(\mathbb{S}^t, \mathbf{m}_{ev}^{t}, \mathbb{S}^{t+1}\right) = -(&w_{ref}\left\|P_{ev}^{t+1} - P_{ev}^{ref,t+1}\right\|_2 \\ &+ w_v\left|v_{ev}^{X,t+1} - v_{ev}^{X,*,t+1}\right| \\ &- w_{ped}\left\|P_{ev}^{t+1} - P_{ped}^{t+1}\right\|_2) \end{aligned} \tag{17}$$

where $P_{ev}^{ref,t}$ is the reference path for the ego vehicle, and $v_{ev}^{x,*,t}$ represents the optimal speed of the ego vehicle in the X-direction at time t. w_{ref},w_v and w_{ped} are the weights of evaluation indexes, respectively. This reward function requires the ego vehicle to balance tracking the reference path, tracking optimal velocity and keeping away from the pedestrian. And the purpose is to maximize this reward at every time step.

When the initial state $\mathbb{S}^0$ is determined, the purpose is to find the optimal policy π^* that could maximize the expect future reward $V^*\left(\mathbb{S}^0\right)$ from the following system state $\mathbb{S}^1, \ldots, \mathbb{S}^{t_{end}}$ by selecting the optimal maneuver $m_{ev}^{*} \in M_{ev}$ at each time step for ego vehicle, which could be considered as a Markov decision process(MDP):

$$V^*\left(\mathbb{S}^0\right) = \max_{\pi \in \Pi} \mathbb{E}\left[\sum_{t=t_0}^{t=t_{end}} \left[\gamma^t r\left(\mathbb{S}^t, \mathbf{m}_{ev}^{t}, \mathbb{S}^{t+1}\right) \middle| \pi\right]\right] \tag{18}$$

where $\gamma \in (0, 1)$ is a discount factor. Generally, the Bellman Optimal Equation is adopted to solve the MDP:

$$V^*\left(\mathbb{S}^t\right) = \max_{\mathbf{m}_{\text{ev}}}(r\left(\mathbb{S}^t, \mathbf{m}_{\text{ev}}^t, \mathbb{S}^{t+1}\right) + \gamma \sum_{\mathbb{S}^{t+1}\in\mathbb{S}_{all}} p\left(\mathbb{S}^{t+1}\middle|\mathbb{S}^t, \mathbf{m}_{\text{ev}}^t\right) V^*\left(\mathbb{S}^{t+1}\right)) \tag{19}$$

And the initial states of the ego vehicle and pedestrian are set as:

$$\delta_{\text{ped}}^0 = \delta_{\text{ev}}^0 = 0\ rad \tag{20}$$

$$\begin{cases} v_{\text{ped}}^{x,0} = 1.2\ m/s \\ v_{\text{ped}}^{y,0} = 0\ m/s \end{cases} \tag{21}$$

$$a_{\text{ped}}^0 = a_{\text{ev}}^0 = 0m\Big/s^2 \tag{22}$$

$$D_{\text{ev2p}}^{Y,0} = Y_{\text{ped}}^0 - Y_{\text{ev}}^0 = 2m \tag{23}$$

where $D_{\text{ev2p}}^{Y,0}$ is the Y-direction deviation distance between the ego vehicle and pedestrian at the initial time. The minimum safe distance, which is defined as $\min D_{\text{safe}}$, is set as $1.5m$ in this paper. Considering the ego vehicle is approaching a pedestrian with stochastic moving, a $0.5m$ offset is added to $D_{\text{ev2p}}^{Y,0}$. The X-direction deviation distance $D_{\text{ev2p}}^{X,0}$ is unspecified, or in other words, it can be any reasonable value for ego vehicle to successfully complete the CA process. Namely, the previous state of the vehicle is supposed to be cruising with a initial velocity v_{ev}^0.

However, a fundamental problem with MDP is that the size of the state space $\mathbb{S}$ and the size of the action space M both can grow quickly due to the high dimension of the space, or due to increasingly fine-grained discretization to approach a continuous representation. Which is referred to as the curse of dimension by Bellman [35]. For the MDP problem addressed in this paper, noticing the reference path in the proposed scenario maintains a straight line, and the optimal speed profile $v_{\text{ev}}^{x,*}$ in Eq.(17) is inaccessible during the solution, the reward function $r\left(\mathbb{S}^t, m_{\text{ev}}^t, \mathbb{S}^{t+1}\right)$ at each time step is replaced by a R that defines the total reward of the whole CA process for simplification:

$$R = W_{\text{ref}} d_{\text{ev2ref}}^{\min} + W_{\text{v}} \bar{v}_{\text{ev}}^X - W_{\text{ped}} d_{\text{ev2ped}}^{\min} \tag{24}$$

where

$$d_{\text{ev2ref}}^{\min} = \min\left\{\left|Y_{\text{ev}}^t - Y_{\text{ev}}^{\text{ref}}\right| \middle| t \in (t_0, t_{\text{end}})\right\} \tag{25}$$

$$\bar{v}_{\text{ev}}^X = \frac{\sum_{i=1}^{end} v_{\text{ev}}^{X,i} \cdot T_s}{t_{\text{end}} - t_0} \tag{26}$$

$$d_{\text{ev2ped}}^{\min} = \min\left\{\left\|P_{\text{ev}}^t - P_{\text{ped}}^t\right\|_2 \middle| t \in (t_0, t_{\text{end}})\right\} \tag{27}$$

where T_s is the sampling time. And when the initial state $\mathbb{S}^0$ is determined, the $V^*\left(\mathbb{S}^0\right)$ is approximated to the maximum value of R:

$$V^*\left(\mathbb{S}^0\right) = \max R \tag{28}$$

Then, instead of searching the optimal policy π^*, it is possible to directly obtain the optimal maneuver profile m_{ev}^* by the total reward R. Combining Eq.(24)- Eq.(28), the first item of function R, which is from Eq.(25), requires the ego vehicle to follow the reference path that is corresponding to the requirement of slight steering. The second item, which is from Eq.(26), gives the average X-direction vehicle speed during the CA process that is corresponding to the requirement of quick passing. And the final item, which is from Eq.(27), is corresponding to the requirement of safe passing.

Due to the above assignments, it is possible to define a feasible profile δ_{ev}^t and $a_{\text{ev}}^{x,t}$ as follows:

Definition 1: Curves δ_{ev}^t and $a_{\text{ev}}^{x,t}$ are feasible if they are l^{-1}-continuity and satisfy conditions (8) - (14). The set of feasible δ_{ev}^t and $a_{\text{ev}}^{x,t}$ are written as $\mathbb{F}_\delta$ and $\mathbb{F}_a$, respectively.

In summary, this paper addressed the following maneuver planning problem:

Problem 1: Given the determinate initial state $\mathbb{S}^0$ and reward function R to calculate the optimal maneuver profile $\mathbf{m}_{\text{ev}}^{*,t}, \forall t \in [t_0, t_{end}]$ which satisfies:

$$\mathbf{m}_{\text{ev}}^* = \underset{\mathbf{m}_{\text{ev}}^t \in (\mathbb{F}_\delta \cap \mathbb{F}_a)}{\arg\max}\ R \quad s.t.\quad Equ.(8) - (14) \tag{29}$$

Considering the vehicle-pedestrian interaction has been thoroughly researched, this paper makes the following assumption:

Assumption 2: Considering $\mathbb{S}^0$ follows conditions (20)-(23) and $\mathbf{m}_{\text{ev}}^t \in (\mathbb{F}_\delta \cap \mathbb{F}_a)$ is a finite set, the transition function $p\left(\mathbb{S}^{t+1}\middle|\mathbb{S}^t, \mathbf{m}_{\text{ev}}^t\right)$ is approximated by an explicit equation that describes a system state $\mathbb{S}^{t+1}$ that reaches from $\mathbb{S}^t$ by ego vehicle taking a specific maneuver $\mathbf{m}_{\text{ev}}^t$:

$$\mathbb{S}^{t+1} = f_{\text{env}}\left(\mathbb{S}^t, \mathbf{m}_{\text{ev}}^t\right) \tag{30}$$

The following section III gives a modified SFM to approximate the dynamic function f_{env}, and section IV gives the solution of optimal maneuver profile m_{ev}^* which is known as **Problem** 1.

III. SFM-BASED DYNAMIC MODEL

As the target scenario is not complex, a explicit dynamic equation f_{env} is used to approximate transition possibility function p, which is defined as **Assumption 2**. It is convenient to calculate the total reward R of Eq.(24), which is essential for solving **Problem 1**, after establishing f_{env}.In the following part, the method of establishing f_{env} will be introduced in detail.

A. SFM-BASED PEDESTRIAN MODEL

In previous researches, when considering vehicle-pedestrian interaction during CA process, the movement of pedestrians was usually considered to be uniform or moving according to given profiles of speed and trajectory. However, in actual

scenarios, pedestrian movement will be affected by different external factors. In complex urban scenarios, behavior of a pedestrian is affected by various types of traffic participants, which in most cases are surrounding pedestrians and vehicles.

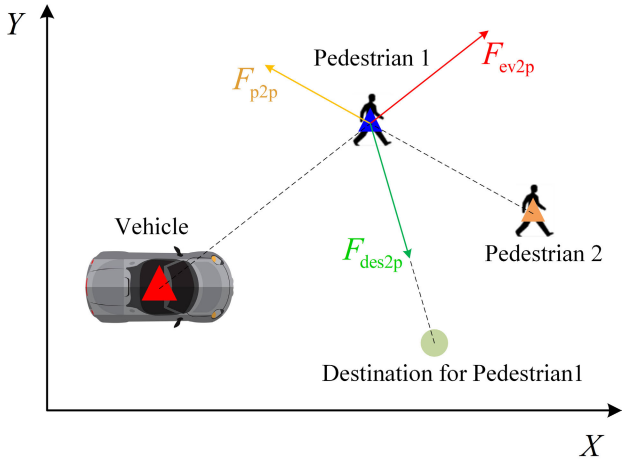

FIGURE 7. SFM-based pedestrian model.

Fig. 7 shows a simple illustration of SFM-based model for pedestrian 1. The pedestrian 1 is affected by surrounding elements which lead to his changing of the path to the destination. These effects can be viewed as some force exerting on the pedestrian 1, such as a repulsive force from vehicle $\mathbf{F}_{\text{ev2p}}$, a repulsive force from other pedestrian 2 $\mathbf{F}_{\text{p2p}}$ and an attractive force from destination $\mathbf{F}_{\text{des2p}}$. However, the interaction force is only based on the current states of the traffic participants which means the historical data is ignored. To some extent, the SFM-based CA process is Markov-like process. So, based on **Assumption** 1, SFM-based dynamic model is suitable in the proposed scenario.

Pedestrians are regarded as a point mass in the social force model, whose dynamic is defined as:

$$\dot{X}_{\text{ped}} = v^X_{\text{ped}} \tag{31}$$

$$\dot{Y}_{\text{ped}} = v^Y_{\text{ped}} \tag{32}$$

$$\dot{v}^X_{\text{ped}} = a^X_{\text{ped}} = \frac{F^{X,t}_{\text{ped}}}{m_{\text{ped}}} \tag{33}$$

$$\dot{v}^Y_{\text{ped}} = a^Y_{\text{ped}} = \frac{F^{Y,t}_{\text{ped}}}{m_{\text{ped}}} \tag{34}$$

where superscript $[X, Y]$ are the components of Cartesian coordinates that belong to the world axis frame. $F^{X,t}_{\text{ped}}$, $F^{Y,t}_{\text{ped}}$ are the total force imposing on pedestrian at current time t in lateral and longitudinal axles, respectively. m_{ped} represents the mass of pedestrian. The total force $\mathbf{F}^t_{\text{ped}}$ at time t, that is formed by $F^{X,t}_{\text{ped}}$ and $F^{Y,t}_{\text{ped}}$, is the summation of multi-source effect:

$$\mathbf{F}^t_{\text{ped}} = \mathbf{F}^t_{\text{ev2p}} + \mathbf{F}^t_{\text{p2p}} + \mathbf{F}^t_{\text{des2p}} + \mathbf{F}^t_{\text{noise}} \tag{35}$$

where $\mathbf{F}^t_{\text{ev2p}}$ represents the force from interaction with vehicle. $\mathbf{F}^t_{\text{des2p}}$ is the force from destination which is simplified in this study as the pedestrian's willingness to keep the initial speed constant. $\mathbf{F}^t_{\text{p2p}}$ is pedestrian-pedestrian interaction force. As this study mainly focuses on designing CA avoidance strategies for vehicle, and the scenario given by Fig. 2 only contains one pedestrian. So, the pedestrian-pedestrian interaction force $\mathbf{F}^t_{\text{p2p}}$ is ignored in this study. Besides, the force cannot fully generalize all factors that may affect the target pedestrian, therefore a Gaussian distribution-based noise $\mathbf{F}^t_{\text{noise}}$ is added to SFM-based pedestrian model for simulating uncertainty.

And components of $\mathbf{F}^t_{\text{ped}}$ are defined as:

$$\mathbf{F}^t_{\text{ev2p}} = f_{\text{exp}}\left(d^t_{\text{ev2p}}, A_{\text{ev2p}}, B_{\text{ev2p}}\right) \text{A}_{\text{sin}}\left(\phi^t_{\text{ev2p}}, \lambda_{\text{ev2p}}\right) \tag{36}$$

$$\mathbf{F}^t_{\text{des 2p}} = \beta_{\text{ev2p}} \cdot \kappa_{\text{des 2p}} \cdot \left(\mathbf{v}^t_{\text{ped}} - \mathbf{v}^0_{\text{ped}}\right) \tag{37}$$

$$\mathbf{F}^t_{\text{noise}} = \kappa_{\text{noi}} \cdot \chi,\ \chi \sim N(\mu, \sigma) \tag{38}$$

where κ_{des2p} is a feedback gain for the destination force, κ_{noi} is a gain for Gaussian based white noise (where $\mu = 0$ and $\sigma = 1$). The other parameters of each force are described as following:

$$f_{\text{exp}} = \text{A}_{\text{ev2p}} \cdot e^{\left(-B_{\text{ev2p}} \cdot d^t_{\text{ev2p}}\right)} \tag{39}$$

This function represents a decaying function that the magnitude of force $\vec{F}^t_{\text{ev2p}}$ decreases monotonically as the distance between the ego pedestrian to the target agent increases. d^t_{ev2p} is a variable representing the distance between the ego pedestrian and the target agent, and A_{ev2p},B^t_{ev2p} are parameters adjusting the characteristics of the decaying relationship:

$$\text{A}_{\text{sin}} = \lambda_{\text{ev2p}} + \left(1 - \lambda_{\text{ev2p}}\right) \frac{1 + \cos\left|\phi^t_{\text{ev2p}}\right|}{2} \tag{40}$$

This function represents anisotropy function that its output is a scalar ranging from 0 to 1, representing how the influence attenuates as the angle between pedestrian's walking direction and his direction to the target agent increases. $\phi^t_{\text{ev2p}} \in \left[-\pi\ \pi\right]$ is a variable representing the interaction angle and λ_{ev2p} is the parameter adjusting the anisotropy characteristics [17].

$$\beta_{\text{ev2p}} = \max\left\{\min\left\{\frac{d^t_{\text{ev2p}} - d^{\text{swi}}_{\text{ped}}}{d^{\text{swi}}_{\text{ped}}}\right\}, 0\right\} \tag{41}$$

This item represents a switch function which allows the pedestrian to switch from mainly focusing on reaching the destination to avoiding the collision with vehicle. d^{swi}_{ped} denotes the switch distance for pedestrian. Besides, the method for calibrating parameters of SFM-based pedestrian model are established in [17].

B. SFM-BASED VEHICLE MODEL

Similar as the definition of SFM-based pedestrian model, the SFM model could also be adopted for a point-mass vehicle

dynamic model, which is a modified version of SF based pedestrian model, shown as Fig.8. It is defined as:

$$\dot{X}_{\text{ev}} = v_{\text{ev}}^{X} \tag{42}$$

$$\dot{Y}_{\text{ev}} = v_{\text{ev}}^{Y} \tag{43}$$

$$\dot{v}_{\text{ev}}^{X} = a_{\text{ev}}^{X} = \frac{F_{\text{ev}}^{X,t}}{m_{\text{ev}}} \tag{44}$$

$$\dot{v}_{\text{ev}}^{Y} = a_{\text{ev}}^{Y} = \frac{F_{\text{ev}}^{Y,t}}{m_{\text{ev}}} \tag{45}$$

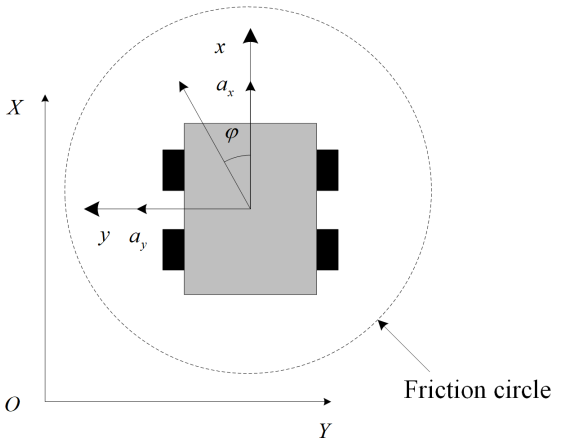

FIGURE 8. Mass point model.

where $F_{\text{ev}}^{X,t}$ and $F_{\text{ev}}^{Y,t}$ are the components of the total force $\mathbf{F}_{\text{ev}}^{t}$ exerted on ego vehicle in $[X, Y]$ direction.

$$\mathbf{F}_{\text{ev}}^{t} = \mathbf{F}_{\text{p2ev}}^{t} + \mathbf{F}_{\text{des2ev}}^{t} + \mathbf{F}_{\text{brake}}^{t} \tag{46}$$

In SFM-based vehicle model, the definition of $\vec{F}_{\text{p2ev}}^{t}$ is similar with that of pedestrian, and the force from destination $\vec{F}_{\text{des2ev}}^{t}$ could be considered as the force that requires vehicle to track the reference trajectory,which are established as following:

$$\mathbf{F}_{\text{p2ev}}^{t} = f_{\text{exp}}\left(d_{\text{p2ev}}^{t}, A_{\text{p2ev}}, B_{\text{p2ev}}\right) \text{A}_{\text{sin}}\left(\phi_{\text{p2ev}}^{t}, \lambda_{\text{p2ev}}\right) \tag{47}$$

$$\mathbf{F}_{\text{des2ev}}^{t} = \beta_{\text{des2ev}} \cdot \kappa_{\text{des2ev}} \cdot \omega_{v}\left(\mathbf{v}_{\text{ev}}^{t} - \mathbf{v}_{\text{ref4ev}}^{t}\right) \cdot \omega_{Y}\left(Y_{\text{ev}}^{t} - Y_{\text{ev}}^{0}\right) \tag{48}$$

where $\mathbf{v}_{\text{ref4ev}}^{t}$ is the reference speed for current time t. ω_v and ω_Y are the weight of tracking current reference speed and the weight of tracking reference path, respectively. As the reference trajectory of ego vehicle in this scenario is a line with constant Y- coordinate, only the current Y- coordinate of ego vehicle is under consideration in tracking reference path. These two types of force are considered as raw force of SFM-based vehicle model.

The new added item $\mathbf{F}_{\text{brake}}^{t}$ is used to provide a force that is generated by vehicle controller to indicate ego vehicle to operate optimal obstacle avoidance maneuvers, which is established as

$$\mathbf{F}_{\text{brake}}^{t} = f\left(Flag, D_{\text{ev2p}}^{X,t}\right) \tag{49}$$

Flag is a Boolean using to judge whether the pedestrian is now crossing the road and $D_{\text{ev2p}}^{X,t}$ is the X-direction distance between the pedestrian and the ego vehicle. This force is considered an artificially applied force.

C. PROBLEM 1 RECONSTRUCTION

The mass point model is adopted for ego vehicle to reduce the influence of its profile on the interaction force as well as simplifying the calculation, which is defined as:

$$\dot{X}_{\text{ev}}^{t} = v_{\text{ev}}^{x,t}\cos\varphi - v_{\text{ev}}^{y,t}\sin\varphi \tag{50}$$

$$\dot{Y}_{\text{ev}}^{t} = v_{\text{ev}}^{x,t}\sin\varphi + v_{\text{ev}}^{y,t}\cos\varphi \tag{51}$$

$$m_{\text{ev}}a_{\text{ev}}^{Y,t} = F_{\text{ev}}^{Y,t} \tag{52}$$

$$m_{\text{ev}}a_{\text{ev}}^{X,t} = F_{\text{ev}}^{X,t} \tag{53}$$

where φ is the yaw angle, and the resultant force on the vehicle tires should satisfy the friction circle constraint:

$$\left(a_{\text{ev}}^{X,t}\right)^2 + \left(a_{\text{ev}}^{Y,t}\right)^2 \leq (k\mu g)^2 \tag{54}$$

where μ is the road friction coefficient and $k \leqslant 1$ is a gain to limit saturation of tire friction.

Considering that SFM model generates force that is exerted on vehicle and causes the changing on vehicle's trajectory, and the force is continues. Therefore, the optimal maneuver $\mathbf{m}_{\text{ev}}^{*}$ is regarded to be determined by initial system state $\mathbb{S}^0$ and the optimal force set $\mathbf{F}_{\text{ev}}^{*}$ according to the definition of SFM-based vehicle model Eq.(42)-(46) and (52), (53). Noticing initial system state $\mathbb{S}^0$ is predetermined and the force $\mathbf{F}_{\text{ev}}^{*}$ is determined by related SFM parameters, the solution of $\mathbf{m}_{\text{ev}}^{*}$ could be transformed into the optimization of those parameters, which is written as Φ_{ev}^{*}, in SFM-based vehicle model with the same constraints Eq.(8)-(14).

As the definition of original SFM-based model (39)-(41) and modified destination force (48), there are 8 parameters that could be optimized which are

(1) Parameters A_{p2ev}, B_{p2ev} of function f_{exp} in force from pedestrian $\mathbf{F}_{\text{p2ev}}^{t}$. A_{p2ev} mainly provides the magnitude of $\mathbf{F}_{\text{p2ev}}^{t}$ and B_{p2ev} indicates rate of decaying in distance;

(2) Parameter λ_{p2ev} of function A_{sin} in $\mathbf{F}_{\text{p2ev}}^{t}$, it mainly indicates rate of decaying in direction;

(3) Parameter κ_{des2ev} of force from destination $\mathbf{F}_{\text{des2ev}}^{t}$, it provides the magnitude of $\mathbf{F}_{\text{des2ev}}^{t}$;

(4) Parameter $d_{\text{ev}}^{\text{swi}}$ of function β_{p2ev}^{i} in $\mathbf{F}_{\text{des2ev}}^{t}$, it determines the switch distance;

(5) Parameters ω_v, ω_Y and $\mathbf{v}_{\text{ref4ev}}^{t}$ of force from destination $\mathbf{F}_{\text{des2ev}}^{t}$, which give the tracking weights and the reference velocity, respectively.

However, if the force from pedestrian $\mathbf{F}_{\text{p2ev}}^{t}$ is equal to zero, the vehicle will keep the initial speed and operate no turning maneuver. It means the ego vehicle maintains the reference trajectory in this research, which results in the force from destination $\mathbf{F}_{\text{des2ev}}^{t}$ will also be zero. So, the decisive parameter that needs to be optimized is A_{p2ev} which mainly provides the magnitude of $\mathbf{F}_{\text{p2ev}}^{t}$. Therefore, in this research,

the optimal A^*_{p2ev} and $v^{X,*}_{\text{ref4ev}}$ are the only two parameters that need to be searched for simplification:

$$\Phi^*_{\text{ev}} = \left[A^*_{\text{p2ev}}, v^{X,*}_{\text{ref4ev}}\right] \tag{55}$$

while other parameters are set as defaults. The calibration and corresponding analysis of all SFM-based vehicle model parameters were elaborated by our another work [42].

So, the initial *Problem 1* is transformed from directly calculating optimal maneuver $\mathbf{m}^*_{\text{ev}}$ to searching the optimal parameters series Φ^*_{ev} for SFM-based vehicle model.

IV. PROPOSED METHOD

A. ANALYSIS OF AVOIDANCE PROCESS

Firstly, the new added artificially applied force, which comes from controller(or strategy) $\mathbf{F}^t_{\text{brake}}$, in SFM-based vehicle model is ignored. The following part describes the optimal raw parameters of SFM-based vehicle model at various vehicle-pedestrian distances. Considering that the initial conditions (defined by Eq.(20)-(23)) of the target scenario do not specify the initial X-direction vehicle-pedestrian distance $D^{X,0}_{\text{ev2p}}$. So, firstly, a PSO-based optimization is employed to determine the relation between Φ^*_{ev} and various $D^{X,0}_{\text{ev2p}}$.

A test scenario is shown by Figure 9. Fixing the initial state $\mathbb{S}^0_{\text{ev}}$ of vehicle and the Y-direction deviation distance between the ego vehicle and the pedestrian $D^{Y,0}_{\text{ev2p}}$. When the pedestrian chooses different X-position (defined as X^i_{ped}) to cross road, it leads to different $D^{X,i}_{\text{ev2p}}$. And this scenario simulates the sudden crossing of a pedestrian under varying $D^{X,0}_{\text{ev2p}}$ when the vehicle is cruising.

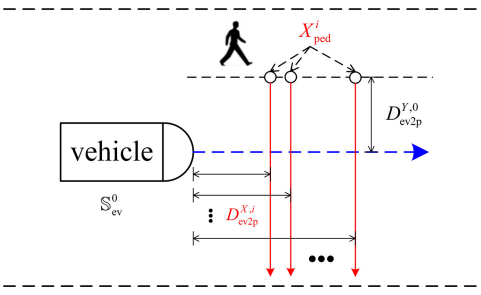

FIGURE 9. Random choices of pedestrian crossing road point.

1) PSO-BASED OPTIMIZATION

PSO is a global search algorithm based on random search that simulates natural biological activities and swarm intelligence. It is well-suited for finding the (near)-optimal solutions to complex systems because it has no special requirements for the continuity of the optimization problem. During the parameters optimization in this study, Simulated Annealing (SA) and adaptive weights/learning rates were adopted based on the basic PSO, which may benefit in overcoming the local minima problem.

A swarm $\Theta_i = (\Theta_{i1}, \Theta_{i2}), i = 1, 2, \ldots, N$ with an initial random speed $v_i = (v_{i1}, v_{i2}), i = 1, 2, \ldots, N$ is defined for PSO initialization to traversal the whole CA process. the performance of each particle Θ_i is evaluated by a cost function. And when iterations of traversal is reached the upper limit or the cost of value function is acceptable, it is considered that the current set Θ is the solution set Θ^*, shown as Figure 10.

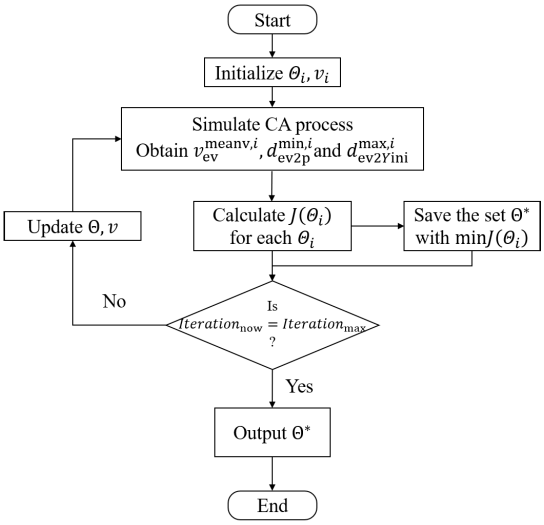

FIGURE 10. Optimization process of SFM parameters and speed for ego vehicle.

In addition, lower bounds and upper bounds were added to Θ_i, which $A^i_{\text{p2ev}} \in [0, 6000]$ and $v^i_{\text{ref4ev}} \in [0, 10]$ to ensure that in the process of calibration, the parameters are not set to unrealistic values. Additionally, the total number of particles in the PSO was set to 40, which is sufficient for the calibration process.

The loss function is defined as

$$J(\Theta_i) = q^{\text{PSO}} \cdot \frac{1}{v^{meanv,i}_{\text{ev}}} + r^{\text{PSO}} \cdot \frac{1}{d^{\text{min},i}_{\text{ev2p}}} + p^{\text{PSO}} \cdot d^{\text{max},i}_{\text{ev2Yini}} \tag{56}$$

where

$$\begin{cases} r^{\text{PSO}} = r^{\text{PSO}}, & d^{\text{min},i}_{\text{ev2p}} \geq \min D_{\text{safe}} \\ r^{\text{PSO}} = L \cdot r^{\text{PSO}}, & d^{\text{min},i}_{\text{ev2p}} < \min D_{\text{safe}} \end{cases} \tag{57}$$

$$d^{\text{min},i}_{\text{ev2p}} = \min\left\{ d^{i,t}_{\text{ev2p}} \middle| t \in (t_0, t_{end}) \right\} \tag{58}$$

$$d^{\text{max},i}_{\text{ev2ref}} = \max\left\{ d^{i,t}_{\text{ev2ref}} \middle| t \in (t_0, t_{end}) \right\} \tag{59}$$

This loss function aims for the ego vehicle to pass pedestrians with minimal steering and deceleration, ensuring a safe avoidance. The r^{PSO} is a very small constant when the $d^{\text{min},i}_{\text{ev2p}}$ is larger than $\min D_{\text{safe}}$, which means the ego vehicle needs a series of optimized parameters to achieve a higher passing speed when the distance is deemed safe. L is a large constant that provides a sufficient cost that the ego vehicle maintains an acceptable, safe distance away from the pedestrian.

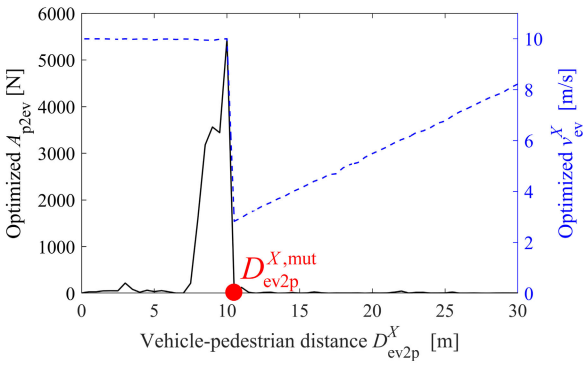

FIGURE 11. The optimal A_{p2ev} and v_{ev} under different D_{ev2p}^X.

Fig. 11 shows the optimized value of A_{p2ev} and v_{ev}^X under different $D_{ev2p}^{X,i}$. The maneuver of the ego vehicle in different $D_{ev2p}^{X,i}$ can be obviously separated to two cases, as shown in Figure 12.

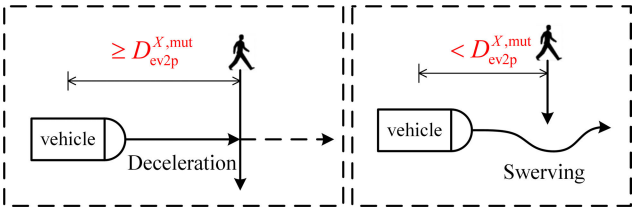

FIGURE 12. Two different avoidance maneuvers of ego vehicle.

2) ANALYSIS OF AVOIDANCE MANEUVERS

When the pedestrian is crossing the road and the vehicle-pedestrian distance is larger than a specific value, which is defined as mutation distance $D_{ev2p}^{X,mut}$, the ego vehicle will be required to decelerate and wait for the pedestrian passing firstly, as shown in Fig. 12. However, when the current interaction distance is extreme short ($< D_{ev2p}^{X,mut}$), the optimal strategy for the ego vehicle to avoid the crossing road pedestrian is to keep a relative higher speed and operate a slight steering maneuver, shown as Fig. 11. Because in such case, the benefits of maintaining high-speed passing are greater than the cost caused by slight steering. This is easily explained when we associate the actions of human drivers in real situations. When the driver finds a pedestrian is crossing road with a distance far from the vehicle, they generally tend to slow down and wait for pedestrian to cross road firstly. Conversely, when the drive approaches a pedestrian who does not have an unpredictable crossing intent, the drive tends to operate turning maneuver with a relative high speed to avoid potential dangers and completes the CA process in a short period of time.

Based on the results from Fig. 11, if it is assumed that a pedestrian is equally likely to cross the road in the future during the approaching process of the ego vehicle, the optimal strategy is to follow the optimal A_{p2ev}^* and $v_{ev}^{X,*}$ based on Fig. 11. The A_{p2ev}^* and $v_{ev}^{X,*}$ are piece-wise polynomial fitted as:

$$v_{ev}^* = f_{fit.v}(D_{ev2p}^X) \tag{60}$$

$$A_{p2ev}^* = f_{fit.A}(D_{ev2p}^X) \tag{61}$$

However, noticing there is mutation for both v_{ev}^* and A_{p2ev}^* in mutation distance $D_{ev2p}^{X,mut}$. Forces can be mutated but not the velocity in the reality. So, when $D_{ev2p}^{X,t}$ is around $D_{ev2p}^{X,mut}$, which could also be roughly considered as the the distance between these two participants decreases from 'long distance' to 'short distance' in Fig. 12, there are two choices for ego vehicle:

(1) *Following strategy*: the ego vehicle keeps deceleration and following the pedestrian until the pedestrian has crossed the road.

However, if

$$-\delta_{ped}^{thr} \leq \delta_{ped}^t \leq \delta_{ped}^{thr}, t \in [t_0, \inf) \tag{62}$$

which means pedestrian keeps walking straightly. However, when $t_{end} = \inf$, the time consumption is unreasonable.

(2)*Overtaking strategy*: the ego vehicle keeps unchanged speed or accelerates to overtake the pedestrian. However, this approach is somewhat risky as it resembles a gambler's strategy. A sudden crossing caused by a careless pedestrian could result in an irreversible collision.

B. PROPOSED METHOD

So, based on the above analysis, the whole CA process is separated into two processes which are approaching process and yielding process, shown as Fig. 13. For convenient, the switch distance here is the same as d_{ev}^{swi}, which function is similar as d_{ped}^{swi} in Eq.(41).

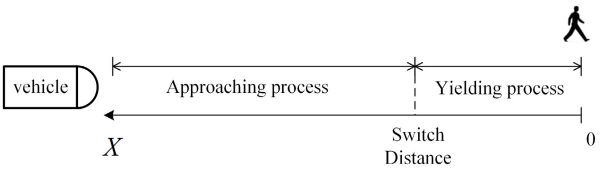

FIGURE 13. Segmentation of CA process.

In approaching process, the ego vehicle will decelerate to a reference longitudinal speed:

$$v_{ref4ev}^{X,t} = v_{ev}^{X,*,t} = f_{fit.v}\left(D_{ev2p}^{X,t}\right) \tag{63}$$

Noticing that $D_{ev2p}^{X,mut} < d_{ev}^{swi}$, the mutation of velocity is avoided in approaching process. In other worlds, the *Following strategy* is adopted in approaching process.

In yielding process, the reference longitudinal speed keeps a constant which is the same as that of switch distance d_{ev}^{swi}:

$$v_{ref4ev}^{X,t}\left(D_{ev2p}^{X,t} \leq d_{ev}^{swi}\right) = v_{ev}^{X,*,swi} = f_{fit.v}\left(d_{ev}^{swi}\right) \tag{64}$$

If the pedestrian does not cross road, this constant speed $v_{\text{ev}}^{X,*,\text{swi}}$ for the ego vehicle in yielding process helps to avoid the problem caused by *Following strategy*.

However, when facing with danger caused by overtaking strategy, it is necessary to calculate a safe speed for the ego vehicle when the pedestrian suddenly crosses the road.

1) PROPOSED METHOD 1 FOR YIELDING PROCESS

In this method, it is assumed that the pedestrian is now crossing the road and will not yield to the ego vehicle, as shown in Fig. 14. In other words, the pedestrian here is considered as a 'careless' individual that the force from the ego vehicle $\vec{F}_{\text{ev2p}}^{t}$ will be ignored by the pedestrian. The pedestrian is considered as a circle whose radius is the minimum safe distance $\min D_{\text{safe}}$ with ego vehicle. Besides, S represents the X-direction distance between outlines of this two participants, which is named safe vehicle-pedestrian distance in X-direction.

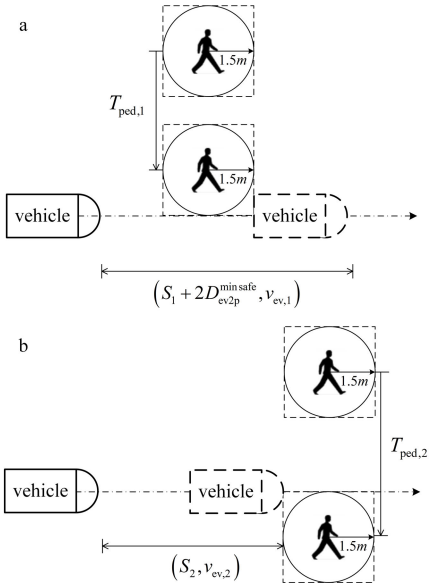

FIGURE 14. Boundary longitudinal speed for ego vehicle.

Then, there are two case for the ego vehicle to yield the pedestrian without turning:

(1) the longitudinal speed of the ego vehicle is fast enough that it has already finished the CA process when the pedestrian reaches the collision point, as shown in Figure 14(a).

(2) the longitudinal speed of ego vehicle is slow enough that the pedestrian has already passed the ego vehicle when the ego vehicle reaches the collision point, as shown in Fig. 14(b).

According to the above analysis, the boundary longitudinal speed could be established as:

$$*20cv_{\text{ev},1} = \frac{S_1 + 2\cdot \min D_{\text{safe}}}{T_{\text{ped},1}} or \quad v_{\text{ev},2} = \frac{S_2}{T_{\text{ped},2}} \tag{65}$$

where $T_{\text{ped},1}$, $T_{\text{ped},2}$ is the time to collision point (TTC) of the pedestrian in case (1) and case (2), respectively. S_1, S_2 are the moving distance of ego vehicle in case (1) and case (2), respectively. $v_{\text{ev},1}$ is the lower boundary of longitudinal speed in case (1) and $v_{\text{ev},2}$ is the upper boundary of case (2), as shown by Fig. 15.

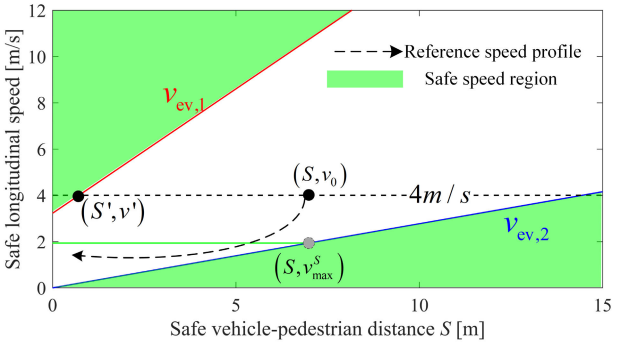

FIGURE 15. Safe longitudinal speed for ego vehicle.

As the definition of S,

$$S^t = D_{\text{ev2p}}^t - \min D_{\text{safe}} \tag{66}$$

When the pedestrian starts crossing the road in current D_{ev2p}^t, the maximum safe speed $v_{\max}^S$ is less than the current speed v_{ev}^t as we consider that acceleration is unreasonable. The ego vehicle needs to decelerate to keep the average longitudinal speed no lager than $v_{\max}^S$. Here we assume acceleration is counter-intuitive for simplification. The following function is established to obtain $a_{\text{ev}}^{x,*}$:

$$v_0 t_1 - \frac{1}{2} a t_1^2 + v_{t_1}(t - t_1) = S \tag{67}$$

$$v_{t_1} = v_0 - a t_1 \tag{68}$$

the v_{ev}^t, S^t and $a_{\text{ev}}^{x,*}$ is rewritten as v_0, S and a for simplification, t_1 is the deceleration time, v_{t_1} is the final speed after deceleration and t is the time when $S = 0$. As the current initial longitudinal speed is relatively small, the effect of jerk of acceleration could be ignored so that it is not under take into consideration for simplification. For pedestrian comfort, a minimum deceleration a is required for ego vehicle:

$$\begin{aligned} \min a &= \frac{S - v_0 t}{\frac{1}{2}t_1^2 - t t_1} \\ s.t. \quad & v_{t_1} \geq 0; \\ & 0 \leq t_1 \leq t \end{aligned} \tag{69}$$

For obtaining minimum a, the derivation of a is

$$a' = \frac{(v_0 t - S)(t_1 - t)}{\left(\frac{1}{2}t_1^2 - t t_1\right)^2} \tag{70}$$

And in this equation,

$$(t_1 - t) \leq 0 \tag{71}$$

$$v_0 t - S = v_0 t - v_{\max}^S t > 0 \tag{72}$$

So,

$$(v_0 t - S)(t_1 - t) \leq 0 \tag{73}$$

which means a is a non-increasing function.

About the limitation factors, the first limitation is $v_{t_1} \geq 0$, which can be transformed into $a \leq \frac{v_0}{t_1}$, which is also equal to

$$\frac{S - v_0 t}{\frac{1}{2}t_1^2 - t t_1} \leq \frac{v_0}{t_1} \tag{74}$$

and can be simplified as $t_1 \leq \frac{2S}{v_0}$.

As $t = \frac{S}{v_{\max}^S}$, the second limitation $0 \leq t_1 \leq t$ can be rewritten as $0 \leq t_1 \leq \frac{S}{v_{\max}^S}$.

So, the limitation factors are final equal to the following form:

$$0 \leq t_1 \leq \min\left(\frac{2S}{v_0}, \frac{S}{v_{\max}^S}\right) \tag{75}$$

Considering a is a non-increasing function,

$$a = \min a \text{ when } t_1 = \min\left(\frac{2S}{v_0}, \frac{S}{v_{\max}^S}\right). \tag{76}$$

And the relation between the optimal deceleration and safe vehicle-pedestrian distance S is shown by Fig. 16.

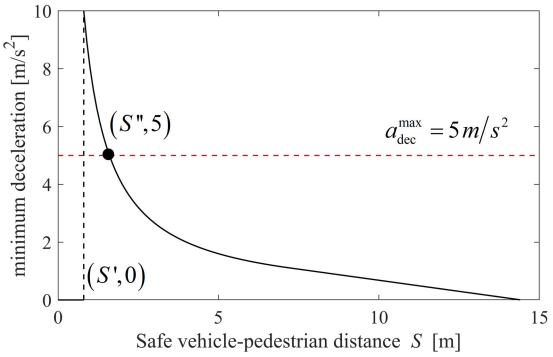

FIGURE 16. Optimal deceleration under different safe distance.

From Fig. 15, When $S < S'$, $v_0 > v_{ev}^1$ always holds, so

$$\min a\left(S < S'\right) = 0 \tag{77}$$

Besides, as the maximum deceleration speed a_{dec}^{max} is set as $5m/s^2$,

$$\min a\left(S \in \left(S', S''\right)\right) > a_{dec}^{max} \tag{78}$$

which means if pedestrian chooses to cross road in this range of distance, deceleration for ego vehicle can not meet the target of avoidance for ego vehicle. The turning is necessary in this case. The final optimal $a_{ev}^{X,*}$ is established as:

$$a_{ev}^{X,*} = \begin{cases} 0, & 0 \leqslant S < S'' \\ \min a, & S \geqslant S'' \end{cases} \tag{79}$$

The reason of $a_{ev}^{X,*} = 0, S \in \left[S', S''\right)$ is that the force $\overrightarrow{F}_{p2ev}$ also owns function of decelerating the ego vehicle. So, when calculating the the optimal A_{p2ev}^* in the range of $S \in \left(S', S''\right)$, the $a_{ev}^{X,*}$ is set to zero for simplification.

The optimal A_{p2ev}^* in SFM-based vehicle model is obtained by balancing the yield speed and deviation distance by PSO with the same loss function Eq.(56). And the results are shown in Fig. 17.

As the turning option for ego vehicle is the only choice when the deceleration is lager than the upper limited, the effective range for A_{p2ev} is when the relative distance belongs to $\left(D_{ev2p}^{X'}, D_{ev2p}^{X''}\right)$, where:

$$\begin{cases} D_{ev2p}^{X'} = S' + \min D_{safe} \\ D_{ev2p}^{X''} = S'' + \min D_{safe} \end{cases} \tag{80}$$

And a fifth order polynomial is used to fit the optimized A_{p2ev},

$$A_{p2ev}^* = f_{fit.A}\left(D_{ev2p}^X\right) \cdot Flag, D_{ev2p}^X \in \left[D_{ev2p}^{X'}, D_{ev2p}^{X''}\right] \tag{81}$$

as the red dot line that is shown in Fig. 17, where $Flag$ is a Boolean that $Flag = 1$ (or $Flag = 0$) means the pedestrian is (or is not) crossing road now, respectively.

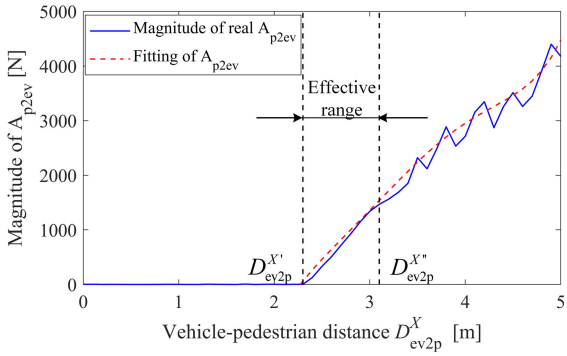

FIGURE 17. Optimal A_{p2ev} under different vehicle-pedestrian distance.

Besides, the optimal deceleration should be transformed into a brake force in SFM-based vehicle model, which is defined as:

$$\mathbf{F}_{brake}^{*,t} = \begin{cases} 0, & D_{ev2p}^{X,t} > d_{ev}^{swi} \\ \left(a_{ev}^{X,*} \cdot mass_{ev} - \vec{F}_{des2ev}^t\right) \cdot Flag, & D_{ev2p}^{X,t} \leq d_{ev}^{swi} \end{cases} \tag{82}$$

where $mass_{ev}$ is the mass of the ego vehicle. Because the calculated a_{dec}^{opt} is the final optimal deceleration of the ego vehicle during the yielding process, the effect of destination force $\mathbf{F}_{des2ev}^t$ should be excluded.

2) PROPOSED METHOD 2 FOR YIELDING PROCESS

In method 1, a consideration was given to a selfish pedestrian who will not yield to the oncoming vehicle during road crossing. When the interaction between the two participants is considered in the yielding process, the optimal operation will be different for ego vehicle. In other words, the pedestrian

here is consider as a 'careful' individual that the force from the ego vehicle $\vec{F}^t_{\text{ev2p}}$ will not be ignored by the pedestrian.

The operation of approaching process for the ego vehicle in this method is the same as method 1. In yielding process, if considering $\mathbf{F}^t_{\text{ev2p}}$, the solution of $a^{x,*}_{\text{ev}}$ will be highly complicated. So, it is transformed into directly search an optimal series of $\mathbf{F}^*_{brake}$ by PSO. The cost function is the same as Eq.(56). The solution here owns two dimensions, and the particle swarm is defined as

$$\Theta_i{}' = \left[A^i_{\text{p2ev}}, \mathbf{F}^i_{\text{brake}}\right] \tag{83}$$

Similarly, lower bounds and upper bounds are added to $\Theta_i{}'$:

$$\begin{cases} A^i_{\text{p2ev}} \in [0, 3000] \\ \mathbf{F}^i_{\text{brake}} \in [0, 4000] \end{cases} \tag{84}$$

The boundaries are used to ensure that the parameters do not exceed unrealistic values during the calibration process. Besides, the total number of particles in the PSO is set to 40, which is sufficient for the calibration. The optimized $\vec{F}_{\text{brake}}$ and A_{p2ev} under different interaction distance D^X_{ev2p} is shown in Fig. 18.

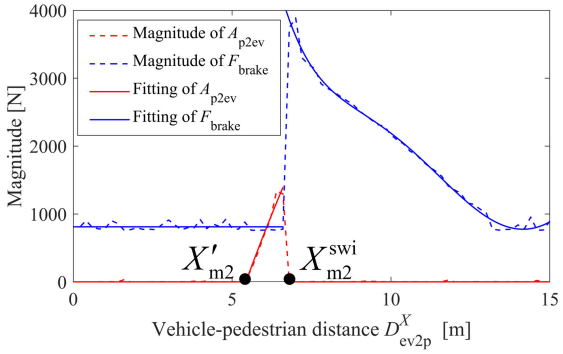

FIGURE 18. Optimal A_{p2ev} and F_{brake} under different vehicle-pedestrian distance.

The fitting of A^*_{p2ev} and $\vec{F}^*_{\text{brake}}$ is written as

$$A^*_{\text{p2ev}} = \begin{cases} f'_{\text{fit.A}}\left(D^X_{\text{ev2p}}\right) \cdot Flag, & D^X_{\text{ev2p}} \in \left[X'_{\text{m2}}, X^{\text{swi}}_{\text{m2}}\right] \\ 0, & D^X_{\text{ev2p}} \notin \left[X'_{\text{m2}}, X^{\text{swi}}_{\text{m2}}\right] \end{cases} \tag{85}$$

$$\mathbf{F}^*_{\text{brake}} = \begin{cases} f_{\text{fit.F}}\left(D^X_{\text{ev2p}}\right) \cdot Flag, & D^X_{\text{ev2p}} \in \left[X^{\text{swi}}_{\text{m2}}, d^{\text{swi}}_{\text{ev}}\right] \\ C_F, & D^X_{\text{ev2p}} \in \left[0, X^{\text{swi}}_{\text{m2}}\right] \end{cases} \tag{86}$$

where $X^{\text{swi}}_{\text{m2}}$ is a certain distance that when $D^X_{\text{ev2p}} \geqslant X^{swi}_{\text{m2}}$, ego vehicle is only required to deceleration. C_F is a constant used to balance the force $\mathbf{F}_{\text{des2ev}}$.

The control logic given by method 2 is similar to that of method 1. Firstly, the ego vehicle is only required to deceleration if D^X_{ev2p} is larger than $X^{\text{swi}}_{\text{m2}}$. Besides, when $D^X_{\text{ev2p}} \in \left[X'_{\text{m2}}, X^{swi}_{\text{m2}}\right)$, the optimal A^*_{p2ev} now is not equal to zero which means turning is the optimal operation choice for the ego vehicle in current stage.

Here, the X'_{m2} is larger than $D^{X''}_{\text{ev2p}}$ in Fig. 17 because that the pedestrian is set to actively avoid the ego vehicle in method 2. So, even if $D^X_{\text{ev2p}} \in \left[D^{X'}_{\text{ev2p}}, D^{X''}_{\text{ev2p}}\right]$, the ego vehicle does not need to turn for maintaining $d_{\text{ev2p}} \geqslant d^{\min}_{\text{ev2p}}$ due to the active yielding of the pedestrian.

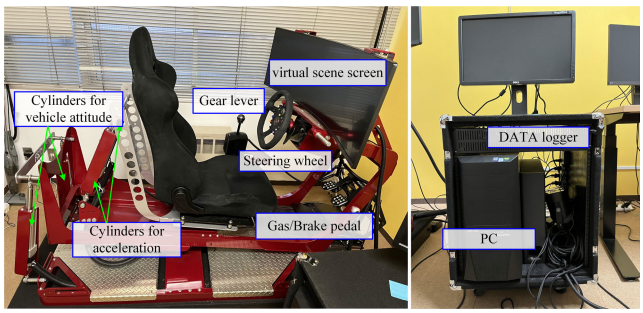

FIGURE 19. View of test bench.

V. BENCH TEST

The view of the test bench is shown in Fig.19. A 4-axis motion stage provided by IROC was adopted in this paper. The vibration, rotation, acceleration, and jerk are generated by 4 cylinders: 2 cylinders provide the pitch angle generated by the gas/brake pedal and the other 2 cylinders provide the roll angle generated by operation of steering wheel. The host computer provides signals of the pedal opening and steering wheel angle generated by Matlab/Simulink and Carmaker.

The control flow of test bench is shown in Fig.20, which is as following:

1.Based on current state information of the ego vehicle $\mathbb{S}^t_{\text{ev}}$ and the pedestrian $\mathbb{S}^t_{\text{ped}}$, generate interacting force $\mathbf{F}^t_{\text{ev2p}}$ and $\mathbf{F}^t_{\text{p2ev}}$;

2.Based on current $D^{X,t}_{\text{ev2p}}$ and the pedestrian moving mode, calculate $A^{*,t}_{\text{ev2p}}$ and $\mathbf{F}^{*,t}_{\text{ev2p}}$ according to Eq.(81) and (82) (or Eq.(85) and (86));

3.Generate $v^{\text{ref},t+1}_{\text{ev}}$ and $a^{x,\text{ref},t+1}_{\text{ev}}$ for next time step $t+1$ according to mass point vehicle model Eq.(50)-(53);

4.Generate corresponding steering wheel angle δ^{t+1}_{ev} and pedal opening p^{t+1}_{ev} by PID for T3R bench.

To verify the reliability of the algorithm under uncertain pedestrian motion, a sequence of discrete times intervals for the pedestrian crossing the road was established at 0.1 second intervals, which is defined as $t^{\text{cro}}_{\text{ped}} = k \cdot t_s, k \in N^+, t_s = 0.1s$. And, if $t \geq t^{\text{cro}}_{\text{ped}}$, the pedestrian will operate crossing road maneuver. The crossing road decision is not known in advance by ego vehicle. The 100 simulation (that means $k = 100$) results of method 1 and 2 under different vehicle-pedestrian distance when pedestrian suddenly crosses road is given by Fig. 21.

From the results, it is obvious that method 2 is a more aggressive strategy due to the active avoidance of the pedestrian, as demonstrated in Fig. 21(d).In Fig. 21(d), the number of times the vehicle's minimum longitudinal

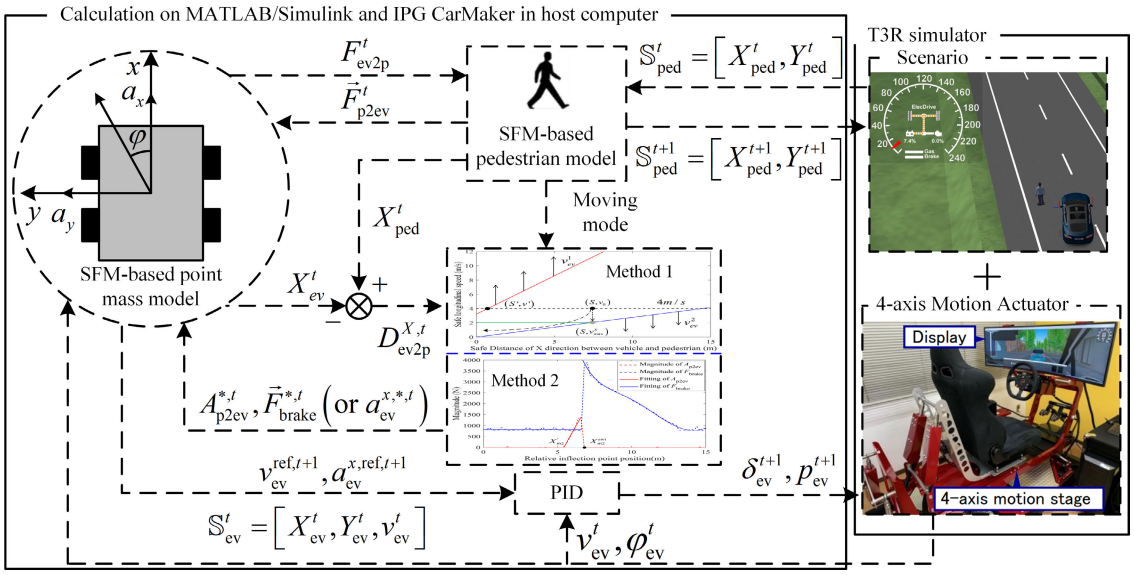

FIGURE 20. Control flow of test bench.

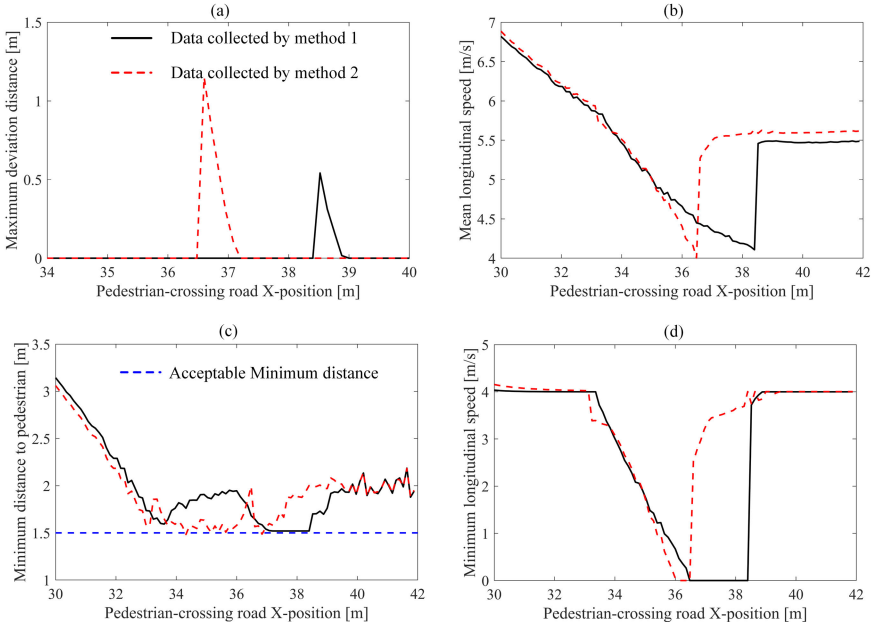

FIGURE 21. Results of method 1 and 2 under successive pedestrian-crossing road X-position:(a) Maximum deviation distance from reference path of ego vehicle;(b) Mean longitudinal speed of ego vehicle;(c) Minimum distance between ego vehicle and pedestrian;(d) Minimum longitudinal speed of ego vehicle.

speed under method 1 equals zero is much higher than that of method 2, meaning that method 1 requires the ego vehicle to decelerate and wait for the pedestrian to pass in most cases while method 2 tends to requires the ego vehicle to avoid the pedestrian with turning maneuver under a relative higher speed. On the other hand, Although the more aggressive strategy of method 2 results in a higher mean longitudinal speed, it also causes a lager maximum deviation distance from the reference path, which are shown by Fig. 21(b) and (a). Besides, both method 1 and method 2 ensure that the ego vehicle safely avoids the pedestrian, as the minimum distance between them is larger than $1.5m$ which is set as the minimum safety distance, as shown in Fig. 21(c).

VI. CONCLUSION

In this work, we introduced a novel SFM-based method with adaptive parameters for the ego vehicle's CA strategy. And the main contribution of this paper can be summarized as:

- The interaction between the ego vehicle and the pedestrian was reasonable simplified as a Markov process, which was supported by real driving data.
- Instead of assessing the risk of the pedestrian crossing or predicting the future pedestrian trajectories, the ego vehicle adopted a force balance-based collision avoidance method, which is simply based on the current state of vehicle-pedestrian interaction system. The SFM-based method eliminates the dangers caused by inaccurate predictions from various environments or individual differences in pedestrians.

By considering pedestrians with two different motion modes, the proposed method was evaluated in a test bench, and the superior results showed that the proposed method helped the ego vehicle maneuver safely, quickly, and with a slight turning yielding to randomly crossing pedestrians.

Due to the proposed scenario and the SFM-based dynamic model, the following future work should be done to improve the current work:

- A more complex scenario,with multiple pedestrians and vehicles should be designed to verify the reliability of proposed method taking into account the interaction between pedestrians and vehicles.
- In the current study, we did not consider the specific causes of pedestrian random movements, but simply used a Gaussian probability model to randomize. In future research, we will carefully explore the causes of the random movements, which may be caused by other traffic elements.
- In this work, pedestrians were simply classified as 'careless' or 'careful'. A more reasonable classification or identification for pedestrian, should be adopted, such as combining pedestrian-aware risk assessment or image recognition.
- In this work, pedestrians were simply classified as 'careless' or 'careful'. A more reasonable classification or identification for pedestrian, should be adopted, such as combining pedestrian-aware risk assessment or image recognition.
- A mass point vehicle model was used for simplification in this work. However, the vehicle shape should be carefully considered, particularly in interacting with moving pedestrian in a low-speed scenarios.

REFERENCES

[1] R. Hajiloo, M. Abroshan, A. Khajepour, A. Kasaiezadeh, and S.-K. Chen, "Integrated steering and differential braking for emergency collision avoidance in autonomous vehicles," *IEEE Trans. Intell. Transp. Syst.*, vol. 22, no. 5, pp. 3167–3178, May 2021.

[2] S. Cheng, L. Li, H.-Q. Guo, Z.-G. Chen, and P. Song, "Longitudinal collision avoidance and lateral stability adaptive control system based on MPC of autonomous vehicles," *IEEE Trans. Intell. Transp. Syst.*, vol. 21, no. 6, pp. 2376–2385, Jun. 2020.

[3] J. Nilsson, A. C. E. Ödblom, and J. Fredriksson, "Worst-case analysis of automotive collision avoidance systems," *IEEE Trans. Veh. Technol.*, vol. 65, no. 4, pp. 1899–1911, Apr. 2016.

[4] Z.-W. Qu, N.-B. Cao, Y.-H. Chen, L.-Y. Zhao, Q.-W. Bai, and R.-Q. Luo, "Modeling electric bike–car mixed flow via social force model," *Adv. Mech. Eng.*, vol. 9, no. 9, Sep. 2017, Art. no. 1687814017719641.

[5] B. Hamilton-Baillie, "Towards shared space," *Urban Design Int.*, vol. 13, no. 2, pp. 130–138, Jun. 2008.

[6] C. Dimmer, "Re-imagining public space," in *Urban Spaces in Japan: Cultural and Social Perspectives*, C. Brumann and E. Schulz, Eds. Evanston, IL, USA: Routledge, 2012, pp. 74–106.

[7] B. Anvari, M. G. H. Bell, A. Sivakumar, and W. Y. Ochieng, "Modelling shared space users via rule-based social force model," *Transp. Res. C, Emerg. Technol.*, vol. 51, pp. 83–103, Feb. 2015.

[8] Y. Saito, R. Yoshimi, S. Kume, X. Shen, A. Yamasaki, R. Matsumi, T. Ito, T. Kinoshita, S. Inoue, T. Shimizu, M. Nagai, H. Inoue, and P. Raksincharoensak, "Effectiveness of a driver assistance system with deceleration control and brake hold functions in stop sign intersection scenarios," *IEEE Trans. Intell. Transp. Syst.*, vol. 23, no. 7, pp. 8747–8758, Jul. 2022.

[9] A. Rasouli and J. K. Tsotsos, "Autonomous vehicles that interact with pedestrians: A survey of theory and practice," *IEEE Trans. Intell. Transp. Syst.*, vol. 21, no. 3, pp. 900–918, Mar. 2020.

[10] C. G. Keller and D. M. Gavrila, "Will the pedestrian cross? A study on pedestrian path prediction," *IEEE Trans. Intell. Transp. Syst.*, vol. 15, no. 2, pp. 494–506, Apr. 2014.

[11] S. Schneider and K. Bengler, "Virtually the same? Analysing pedestrian behaviour by means of virtual reality," *Transp. Res. F, Traffic Psychol. Behav.*, vol. 68, pp. 231–256, Jan. 2020.

[12] X. Shen and P. Raksincharoensak, "Pedestrian-aware statistical risk assessment," *IEEE Trans. Intell. Transp. Syst.*, vol. 23, no. 7, pp. 7910–7918, Jul. 2022.

[13] K. Saleh, M. Hossny, and S. Nahavandi, "Intent prediction of pedestrians via motion trajectories using stacked recurrent neural networks," *IEEE Trans. Intell. Vehicles*, vol. 3, no. 4, pp. 414–424, Dec. 2018.

[14] D. Helbing and P. Molnár, "Social force model for pedestrian dynamics," *Phys. Rev. E, Stat. Phys. Plasmas Fluids Relat. Interdiscip. Top.*, vol. 51, no. 5, pp. 4282–4286, May 1995.

[15] T. Kretz, J. Lohmiller, and P. Sukennik, "Some indications on how to calibrate the social force model of pedestrian dynamics," *Transp. Res. Rec., J. Transp. Res. Board*, vol. 2672, no. 20, pp. 228–238, Dec. 2018.

[16] C. Dias, M. Iryo-Asano, H. Nishiuchi, and T. Todoroki, "Calibrating a social force based model for simulating personal mobility vehicles and pedestrian mixed traffic," *Simul. Model. Pract. Theory*, vol. 87, pp. 395–411, Sep. 2018.

[17] D. Yang, Ü. Özgüner, and K. Redmill, "A social force based pedestrian motion model considering multi-pedestrian interaction with a vehicle," *ACM Trans. Spatial Algorithms Syst.*, vol. 6, no. 2, pp. 1–27, Jun. 2020.

[18] S. Huang, R. S. H. Teo, and K. K. Tan, "Collision avoidance of multi unmanned aerial vehicles: A review," *Annu. Rev. Control*, vol. 48, pp. 147–164, 2019.

[19] R. Isermann, R. Mannale, and K. Schmitt, "Collision-avoidance systems PRORETA: Situation analysis and intervention control," *Control Eng. Pract.*, vol. 20, no. 11, pp. 1236–1246, Nov. 2012.

[20] S. Lefèvre, A. Carvalho, and F. Borrelli, "A learning-based framework for velocity control in autonomous driving," *IEEE Trans. Autom. Sci. Eng.*, vol. 13, no. 1, pp. 32–42, Jan. 2016.

[21] P. Raksincharoensak, T. Hasegawa, and M. Nagai, "Motion planning and control of autonomous driving intelligence system based on risk potential optimization framework," *Int. J. Automot. Eng.*, vol. 7, no. AVEC14, pp. 53–60, 2016.

[22] P. Falcone, F. Borrelli, J. Asgari, H. E. Tseng, and D. Hrovat, "Predictive active steering control for autonomous vehicle systems," *IEEE Trans. Control Syst. Technol.*, vol. 15, no. 3, pp. 566–580, May 2007.

[23] S. Cheng, L. Li, Y.-G. Liu, W.-B. Li, and H.-Q. Guo, "Virtual fluid-flow-model-based lane-keeping integrated with collision avoidance control system design for autonomous vehicles," *IEEE Trans. Intell. Transp. Syst.*, vol. 22, no. 10, pp. 6232–6241, Oct. 2021.

[24] A. Balachandran, M. Brown, S. M. Erlien, and J. C. Gerdes, "Predictive haptic feedback for obstacle avoidance based on model predictive control," *IEEE Trans. Autom. Sci. Eng.*, vol. 13, no. 1, pp. 26–31, Jan. 2016.

[25] Y. Zhang, X. Shen, and P. Raksincharoensak, "Automated Vehicle's overtaking maneuver with yielding to oncoming vehicles in urban area based on model predictive control," *Appl. Sci.*, vol. 11, no. 19, p. 9003, Sep. 2021.

[26] M. Duguleana, F. G. Barbuceanu, A. Teirelbar, and G. Mogan, "Obstacle avoidance of redundant manipulators using neural networks based reinforcement learning," *Robot. Comput. Integr. Manuf.*, vol. 28, no. 2, pp. 132–146, Sep. 2011.

[27] A. Chakravarthy and D. Ghose, "Generalization of the collision cone approach for motion safety in 3-D environments," *Auto. Robots*, vol. 32, no. 3, pp. 243–266, Apr. 2012.
[28] D. Yang and Ü. Özgüner, "Combining social force model with model predictive control for Vehicle's longitudinal speed regulation in pedestrian-dense scenarios," 2019, *arXiv:1907.05178*.
[29] X. Shen and P. Raksincharoensak, "Statistical models of near-accident event and pedestrian behavior at non-signalized intersections," *J. Appl. Statist.*, vol. 49, no. 15, pp. 4028–4048, Nov. 2022.
[30] X. Shen, X. Zhang, T. Ouyang, Y. Li, and P. Raksincharoensak, "Cooperative comfortable-driving at signalized intersections for connected and automated vehicles," *IEEE Robot. Autom. Lett.*, vol. 5, no. 4, pp. 6247–6254, Oct. 2020.
[31] J. Bertram, P. Wei, and J. Zambreno, "A fast Markov decision process-based algorithm for collision avoidance in urban air mobility," *IEEE Trans. Intell. Transp. Syst.*, vol. 23, no. 9, pp. 15420–15433, Sep. 2022.
[32] Abhishek, M. A. A. Boon, M. Mandjes, and R. Núñez-Queija, "Congestion analysis of unsignalized intersections: The impact of impatience and Markov platooning," *Eur. J. Oper. Res.*, vol. 273, no. 3, pp. 1026–1035, Mar. 2019.
[33] J. Shin and M. Sunwoo, "Vehicle speed prediction using a Markov chain with speed constraints," *IEEE Trans. Intell. Transp. Syst.*, vol. 20, no. 9, pp. 3201–3211, Sep. 2019.
[34] C. Mao, L. Bao, S. Yang, W. Xu, and Q. Wang, "Analysis and prediction of Pedestrians' violation behavior at the intersection based on a Markov chain," *Sustainability*, vol. 13, no. 10, p. 5690, May 2021.
[35] R. Bellman, "Dynamic programming," *Science*, vol. 153, nos. 37–31, pp. 34–37, 1966.
[36] S. Petre and R. L. Moses, *Spectral Analysis of Signals*, vol. 452. Upper Saddle River, NJ, USA: Prentice-Hall, 2005.
[37] J. Feng, C. Wang, C. Xu, D. Kuang, and W. Zhao, "Active collision avoidance strategy considering motion uncertainty of the pedestrian," *IEEE Trans. Intell. Transp. Syst.*, vol. 23, no. 4, pp. 3543–3555, Apr. 2022.
[38] M. Ammour, R. Orjuela, and M. Basset, "A MPC combined decision making and trajectory planning for autonomous vehicle collision avoidance," *IEEE Trans. Intell. Transp. Syst.*, vol. 23, no. 12, pp. 24805–24817, Dec. 2022.
[39] J. Liu, P. Jayakumar, J. L. Stein, and T. Ersal, "Combined speed and steering control in high-speed autonomous ground vehicles for obstacle avoidance using model predictive control," *IEEE Trans. Veh. Technol.*, vol. 66, no. 10, pp. 8746–8763, Oct. 2017.
[40] H. M. Fahmy, M. A. A. E. Ghany, and G. Baumann, "Vehicle risk assessment and control for lane-keeping and collision avoidance at low-speed and high-speed scenarios," *IEEE Trans. Veh. Technol.*, vol. 67, no. 6, pp. 4806–4818, Jun. 2018.
[41] S. Na, H. Niu, B. Lennox, and F. Arvin, "Bio-inspired collision avoidance in swarm systems via deep reinforcement learning," *IEEE Trans. Veh. Technol.*, vol. 71, no. 3, pp. 2511–2526, Mar. 2022.
[42] Y. Zhang, X. Shen, and P. Raksincharoensak, "Study on collision avoidance strategies based on social force model considering stochastic motion of pedestrians in mixed traffic scenario," *J. Robot. Mechatronics*, vol. 35, no. 2, pp. 240–254, Apr. 2023.

YAN ZHANG received the master's degree in mechanical engineering from the China University of Geoscience, Beijing, China, in 2020. He is currently pursuing the Ph.D. degree with the Graduate School of Engineering, Tokyo University of Agriculture and Technology. He had research stays with the School of Vehicle and Mobility, Tsinghua University. His research interests include vehicle dynamic control, numerical methods for optimization, model predictive control, and neural networks approximate approaches.

XINGGUO ZHANG received the Ph.D. degree in engineering from Akita Prefectural University, in 2015. He was an Assistant Professor with the Department of Information System Engineering, Akita Prefectural University. Since 2019, he has been an Assistant Professor with the Tokyo University of Agriculture and Technology (TUAT). His research interests include computer vision, virtual reality, and traffic safety assistance technologies.

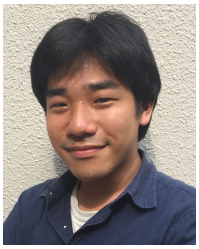

YOHEI FUJINAMI received the B.S., M.S., and Ph.D. degrees in engineering from the Tokyo University of Agriculture and Technology (TUAT), Tokyo, Japan, in 2016, 2017, and 2021, respectively. From 2019 to 2021, he was a Research Fellowships for Young Scientist with the Japan Society for the Promotion of Science. Since 2021, he has been an Assistant Professor with the Department of Mechanical Systems Engineering, TUAT. His research interests include vehicle control and active safety for advanced driver assistance systems and automated driving systems, intersection safety, driver-vehicle interaction, and human–machine interface. He has received many awards, including the Hatakeyama Award from JSME, in 2016, and the Best Paper Award, the Finalist for Best Paper Award, and the Best Presentation Award from the International Symposium FAST-zero, in 2017, 2021, and 2023, respectively.

PONGSATHORN RAKSINCHAROENSAK received the Ph.D. degree in engineering from the Tokyo University of Agriculture and Technology (TUAT), in 2005. After that, he has been an Assistant Professor with TUAT, since 2005, where he has been a Full Professor with the Department of Mechanical Systems Engineering, since 2019. His research interests include vehicle dynamics and control in the context of active safety, handling dynamics, collision avoidance, driver-vehicle interaction, and energy efficiency. He is also the General Secretariat of AVEC Board and a member of technical committee in vehicle dynamics of Society of Automotive Engineers of Japan (JSAE). He received many academic awards from JSAE, International Symposium AVEC, FAST-zero, FISITA World Congress, Japan Society of Mechanical Engineers (JSME), and Masao Horiba.